frontiers | Frontiers in Physics

TYPE Original Research
PUBLISHED 21 October 2022
DOI 10.3389/fphy.2022.1033767

OPEN ACCESS

EDITED BY
Ping Wang,
Barrow Neurological Institute (BNI), United States

REVIEWED BY
Yuxi Pang,
University of Michigan, United States
Weitian Chen,
The Chinese University of Hong Kong, China

*CORRESPONDENCE
Tao Jin,
taj6@pitt.edu

SPECIALTY SECTION
This article was submitted to Medical Physics and Imaging, a section of the journal Frontiers in Physics

RECEIVED 31 August 2022
ACCEPTED 10 October 2022
PUBLISHED 21 October 2022

CITATION
Chung JJ and Jin T (2022), Correction of the post-irradiation T_1 relaxation effect for chemical exchange-sensitive MRI: A phantom study. *Front. Phys.* 10:1033767. doi: 10.3389/fphy.2022.1033767

Correction of the post-irradiation T_1 relaxation effect for chemical exchange-sensitive MRI: A phantom study

Julius Juhyun Chung and Tao Jin*

Department of Radiology, University of Pittsburgh, Pittsburgh, PA, United States

Purpose: In many pulse sequences of chemical exchange-sensitive MRI including multi-slice chemical exchange saturation transfer (CEST) or chemical exchange sensitive spin-lock (CESL), there is a finite time delay between the irradiation preparation and the imaging acquisition, during which the T_1-relaxation reduces the chemical exchange contrast and affects the accuracy for volumetric imaging. We propose a simple post-acquisition method to correct this contamination.

Methods: A simple formula was derived to evaluate the cross-slice T_1-relaxation contamination in multi-slice echo-planar imaging (EPI) after the irradiation preparation. CEST and CESL experiments were performed on phantoms to examine the accuracy of this approach.

Results: Theoretical derivation showed that the cross-slice T_1-relaxation contamination in multi-slice EPI imaging can be corrected by the signals of each slice at a parameter that suppresses the signal, e.g., at the water frequency for CEST, or with very long spin-lock pulse for CESL. This formula was confirmed by the results of phantom experiments, for both long and short irradiation durations with and without a steady-state, respectively. To minimize the effect of B_0 inhomogeneity in the CEST experiment, a more accurate measurement of the signal at water frequency can be achieved with a higher pulse power and shorter duration.

Conclusion: We proposed and validated a simple approach to correct the cross-slice T_1-relaxation effect, which can be applied to volumetric CEST and CESL studies acquired by multi-slice EPI, or other imaging modalities with similar T_1-relaxation contamination.

KEYWORDS

CEST, CESL, multi-slice, T1-relaxation, post-irradiation delay

Introduction

Chemical exchange saturation transfer (CEST) MRI is an emerging molecular imaging technique that can measure certain amounts of biomolecules with labile protons, including glucose, glycogen, amino acids, creatine, and phosphocreatine, as well as exchange rate-related environmental parameters such as pH, temperature, and the concentration of exchange catalysts [1–6]. Due to its versatility, CEST has shown great potential in the study of many diseases such as tumor, stroke, muscle pathology, cartilage and spinal cord injuries, and neurodegenerations [5–25]. In CEST, the labile proton of the biomolecule of interest is usually saturated by an irradiation module during which the bulk water signal is reduced due to the chemical exchange process, and the water magnetization is measured by an imaging module. To avoid the T_1-relaxation effect and fully capture the water magnetization, the post-irradiation delay, i.e., the time delay between the irradiation module and the k-space center of the imaging module, should be minimized.

CEST measures the Z-magnetization of the bulk water and is suitable for studies where the direct water saturation effect is small, e.g., the nutation frequency of the saturation pulse is much smaller than the chemical shift difference between the labile proton and water. In contrast, CESL is another chemical exchange-sensitive MRI technique that images the whole magnetization rather than the Z-component [26–29], and therefore, can be applied to studies where the direct water saturation is large, or even on the resonance of the water frequency. In on-resonance CESL [9, 30], the water magnetization after a spin-lock pulse is in the X-Y plane. For multi-slice imaging, it is often beneficial to flip the magnetization back to the *Z*-axis because the T_1-relaxation of water along the *Z*-axis is much slower than the T_2-relaxation in the X-Y plane.

A common imaging readout method for CEST and CESL MRI is EPI where the post-irradiation delay is negligible for single slice imaging. However, in multi-slice EPI, T_1-relaxation may contaminate the chemical exchange-sensitive signals for the slices acquired after the first slice, especially for the latter slices if the post-irradiation delay time is not negligible as compared to T_1. To minimize this cross-slice T_1-relaxation effect, post-processing using a T_1 map to compensate for the relaxation effect on CEST contrast has been reported [31], which needs a separate acquisition of the T_1 map and would thus lengthen the scan time. A similar T_1-relaxation effect is present in the multi-slice fast spin-echo sequence, and a combination of primary saturation and secondary saturation pulses has been proposed to compensate for this effect [16, 32], however, the choice of primary and secondary saturation may depend on pulse power and tissue properties, therefore careful calibration may be necessary. For multi-slice spin-lock studies, the T_1 contamination in the $T_{1\rho}$-weighted image may be eliminated by an RF cycling technique where the longitudinal magnetization is inverted immediately after alternate spin-lock preparation [33].

In this work, we propose a simple post-acquisition correction method to compensate for the relaxation effect which can be used in multi-slice CEST or CESL MRI, and validate the method by phantom experiments. Part of the results has been reported in ISMRM 2020 [34].

Material and methods

Theory

Assuming the delay between the end of irradiation and the beginning of the acquisition of the *i*th slice is t_{delay} (i) in a multi-slice CEST experiment, the saturated signal of the *i*th slice acquired at an RF offset of Ω can be expressed as

$$S_{sat}(\Omega, i) = S_0 + \left\{S_{sat}^{corr}(\Omega, i) - S_0\right\} \cdot e^{-t_{delay}(i)/T_1} \tag{1}$$

where S_0 is the fully relaxed signal, and S_{sat}^{corr} is the saturated signal after the T_1 relaxation effect is corrected, or the ideal case when the T_1 relaxation effect is minimal, i.e., $t_{delay} = 0$, which is approximately the case for the first slice. At an offset of $\Omega = 0$ (i.e., the water frequency), the water magnetization is fully saturated so that the signal in the absence of the T_1 relaxation effect should be zero, i.e., $S_{sat}^{corr}(\Omega = 0, i) = 0$. Thus

$$\begin{aligned} S_{sat}(\Omega = 0, i) &= S_0 + \left\{S_{sat}^{corr}(\Omega = 0, i) - S_0\right\} \cdot e^{-\left[\frac{t_{delay}(i)}{T_1}\right]} \\ &= S_0\left(1 - e^{-\left[\frac{t_{delay}(i)}{T_1}\right]}\right) \end{aligned} \tag{2}$$

This signal is only related to T_1 and t_{delay}(i), and can fully account for the T_1 recovery during the post-irradiation delay. Combine Eqs 1, 2 to eliminate the exponential term, we have

$$S_{sat}^{corr}(\Omega, i)\Big/S_0 = \frac{S_{sat}(\Omega, i)/S_0 - S_{sat}(\Omega = 0, i)/S_0}{1 - S_{sat}(\Omega = 0, i)/S_0} \tag{3}$$

Note the correction factor used here is

$$\frac{S_{sat}(\Omega = 0, i)}{S_0} = 1 - e^{-\left[\frac{t_{delay}(i)}{T_1}\right]} \approx \frac{t_{delay}(i)}{T_1} \tag{4}$$

when t_{delay} (i) << T_1. The asymmetric magnetization transfer ratio (MTR_{asym}) has been widely used to measure the CEST contrast, which is defined as

$$MTR_{asym}(\Omega) = \frac{S_{sat}(-\Omega) - S_{sat}(\Omega)}{S_0} \tag{5}$$

From Eq. 3, the T_1 relaxation-corrected MTR_{asym} can be derived as

$$MTR_{asym}^{corr}(\Omega, i) = \left\{S_{sat}^{corr}(-\Omega, i) - S_{sat}^{corr}(\Omega, i)\right\}\Big/ S_0 = \frac{MTR_{asym}(\Omega, i)}{1 - S_{sat}(\Omega = 0, i)/S_0} \quad (6)$$

Eqs 3, 4 show that for both the Z-spectrum and the MTR_{asym} spectrum, the T_1-relaxation effect of multi-slice imaging can be easily corrected using the signals acquired from each slice at $\Omega = 0$. Another index to describe the CEST contrast is the difference between the CEST signal at a specific frequency and a baseline with minimal CE signal. The latter can be obtained by model fitting, or by a specifically designed saturation scheme, e.g., a low duty cycle saturation pulse train in the ASEF approach [40]:

$$\Delta S_{sat}(\Omega, i)\Big/ S_0 = \left\{S_{sat}^{baseline}(\Omega, i) - S_{sat}(\Omega, i)\right\}\Big/ S_0 \quad (7)$$

Similarly, we can get

$$\Delta S_{sat}^{corr}(\Omega, i)\Big/ S_0 = \frac{\Delta S_{sat}(\Omega, i)/S_0}{1 - S_{sat}(\Omega = 0, i)/S_0} \quad (8)$$

The same correction approach can be applied to a CESL experiment with a finite spin-lock time (TSL), similar to the derivation above. A very long spin-lock time, e. g, five times the $T_{1\rho}$ value, can be used to suppress the CESL signal, $S_{CESL}^{corr}(TSL = 5T_{1\rho}, i) = 0$. Thus, we have

$$S_{CESL}^{corr}(TSL, i)\Big/ S_0 = \frac{S_{CESL}(TSL, i)\Big/ S_0 - S_{CESL}\Big(TSL = 5T_{1\rho}, i\Big)\Big/ S_0}{1 - S_{CESL}\Big(TSL = 5T_{1\rho}, i\Big)\Big/ S_0} \quad (9)$$

By analogy with the CEST case, the chemical exchange sensitive contrast in a CESL experiment can also be obtained as:

$$\Delta S_{CESL}(TSL, i)\Big/ S_0 = \left\{S_{CESL}^{baseline}(TSL, i) - S_{CESL}(TSL, i)\right\}\Big/ S_0 \quad (10)$$

where the baseline indicates the signal with minimal CE effect. This can be obtained by a spin-lock pulse with a nutation frequency much higher than the chemical exchange rate of interest, such as >4,000 Hz as reported in recent studies [35, 36]. We can also get

$$\Delta S_{CESL}^{corr}(TSL, i)\Big/ S_0 = \frac{\Delta S_{CESL}(TSL, i)/S_0}{1 - S_{CESL}\Big(TSL = 5T_{1\rho}, i\Big)\Big/ S_0} \quad (11)$$

For both CEST and CESL, the correction term is a signal that is fully suppressed at the first slice. Thus, the $S_{sat}(\Omega = 0, i)$ term can also be used for the correction of CESL data to replace the $S_{CESL}(TSL = 5T_{1\rho}, i)$ term in Eqs 8, 10, if all the other imaging parameters are kept the same, such as the repetition time (TR) and echo time (TE). Note that the formula above is independent of the irradiation duration or TR, thus, the correction approach is fully applicable to cases of both CEST and CESL experiments where TR is not sufficiently long for water magnetization to fully relax before the next saturation, as well as CEST experiments where saturation pulse duration is not long enough to achieve a steady state.

MRI experiments

Phantom experiments were performed on a 9.4 T Bruker system at room temperature. A 4.0-cm inner diameter quadrature volume coil provided RF transmission and detection. After the volume of interest was shimmed, a B_0 map was obtained by the WASSR method, and a T_1 map was acquired using an inversion-recovery pulse sequence.

Three phantom experiments were performed:

1) 40 mM of creatine was dissolved in 1× phosphate-buffered saline (PBS) and titrated to pH = 7.4, with and without the addition of 0.15 mM $MnCl_2$ to reduce the water T_1 and T_2 relaxation times. CEST Z-spectra was acquired by a 2 μT pulse with RF offset ranging from 7 ppm to −7 ppm. The duration of saturation pulse is T_{sat} = 8 s, and the repetition time between two consecutive images of the same slice is TR = 13 s. The post-saturation delay t_{acq} was set to 50 ms or 100 ms for each slice.
2) 20% of bovine serum albumin (BSA) was dissolved in PBS, titrated to pH = 7.0, and heated to 75°C for 15 min. This heating process can only denature part of the BSA so that the resulting phantom will be a mixture of mobile and immobile proteins, which is similar to the tissue. CEST Z-spectra was acquired by a 1.5 μT pulse, with RF offset ranging from 7 ppm to −7 ppm. To confirm that our correction method applies to the transient state, a short T_{sat} of 2 s and TR = 4 s was used. In addition, the spectra near the water resonance were measured with 0.8 μT and 5 s pulse, and a 3 μT and 1 s pulse to compare the susceptibility of the correction factor to B_0 shift. The post-saturation delay t_{acq} was set to 100 ms for each slice.
3) For the 20% BSA phantom, CESL data were acquired using an on-resonance spin-lock sequence, where the spin-lock time (TSL) was varied from 0 to 100 ms. In addition, an image with TSL = 300 ms was used for correction following Eq. 8. Data were acquired for two repetition times of TR = 4 and 8 s, and t_{acq} of 126 ms for each slice.

Immediately after the irradiation preparation, a single-shot spin-echo EPI was used to acquire five slices. Other imaging parameters are 64 × 64 matrix size, 4 × 4 cm^2 field of view, 0.6-mm or 1.0 mm slice thickness with a 0.2 mm gap, echo time = 25 ms. Quantitative data were analyzed based on the region of interest (ROI), where only pixels with a B_0 shift of less than 10 Hz were included.

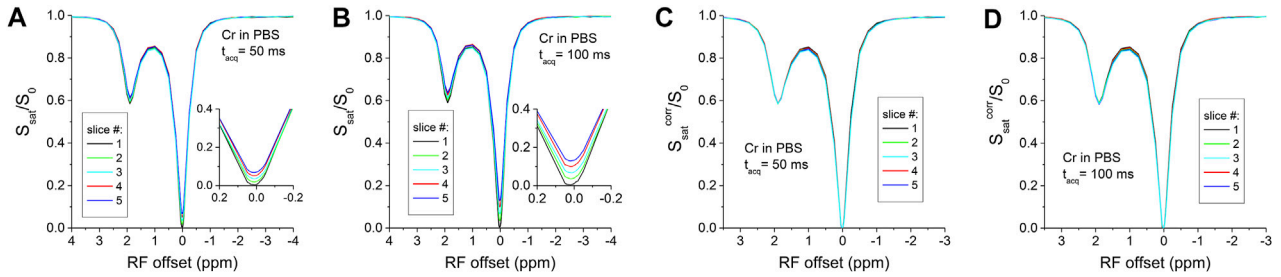

FIGURE 1
Multi-slice CEST Z-spectra of creatine in PBS. The raw Z-spectra show small difference of a few percent among the five slices with t_{acq} = 50 ms **(A)**, and the difference becomes larger with a longer t_{acq} of 100 ms **(B)**. The T_1-relaxation effects can be clearly seen near the water frequency in the Insets. **(C,D)** These differences can be satisfactorily corrected by Eq. 3, leading to overlapping Z-spectra for the five slices.

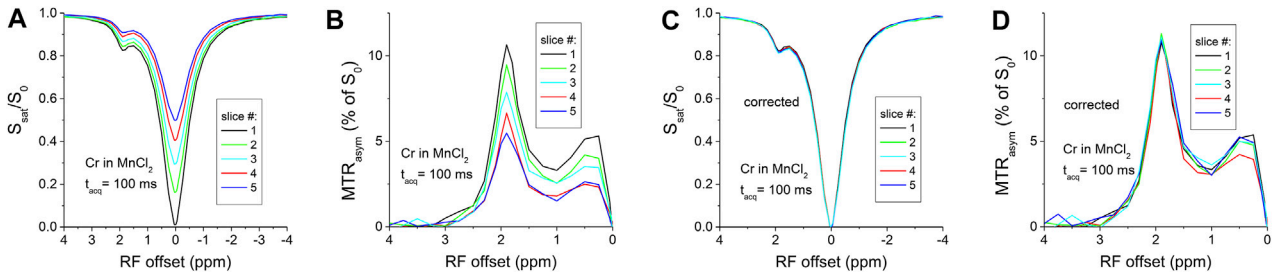

FIGURE 2
Multi-slice CEST MRI of creatine in PBS with $MnCl_2$. The T_1-relxation effect is very significant with t_{acq} = 100 ms in both the Z-spectra **(A)** and the MTR_{asym} spectra **(B)**, which can be satisfactorily corrected by Eqs 3, 6, respectively, leading to overlapping spectra for the five slices **(C,D)**.

Results

Figure 1A shows the Z-spectra of creatine in PBS with t_{acq} = 50 ms. The cross-slice T_1-relaxation effect leads to a small difference in the Z-spectra of the five slices. Due to the relative long T_1 of 2.88 s, the largest delay after saturation is t_{delay} = 200 ms for the fifth slice, which is 7% of the T_1 value. Indeed, the residue signal detected at the water resonance with slice number and reaches a ~7% for the fifth slice (Inset), in good agreement with Eq. 4. For a longer t_{acq} of 100 ms, the T_1-relaxation effect is more significant (Figure 1B), and the residue signal detected at the water resonance reaches a ~14% for the fifth slice (Inset), doubling the value for t_{acq} = 50 ms. After correction with Eq. 3, the Z-spectra for all slices overlap very well for both t_{acq} = 50 and 100 ms (Figures 1C,D). The addition of 0.15 mM $MnCl_2$ shortens the T_1 of the creatine phantom to 0.65 s so that the cross-slice T_1-relaxation effect is amplified. With t_{acq} = 100 ms, there are large distinctions among the Z-spectra (Figure 2A) and the MTR_{asym} (Figure 2B) spectra measured from five slices. The peak of MTR_{asym} at 1.9 ppm for the last slice is reduced by 48% as compared to the first slice (#5 *versus* #1). Using the data at Ω = 0, the Z-spectra and the MTR_{asym} spectra (Figures 2C,D) from the five slices can be corrected well with Eqs 3, 5, respectively.

Figure 3A shows the cross-slice T_1-relaxation effect in a BSA phantom heated to 75°C. This phantom is closer to *in vivo* tissue due to the presence of both mobile and immobile protein, as shown by the CEST and NOE signal dips at 2.8 ppm, −3.5 ppm, and the magnetization transfer (MT) effect at larger offsets (i.e., 6.5 ppm), and the separation between slices can be clearly seen for the whole −7 to 7 ppm range (Figure 3A). With a T_1 value of 1.9 s and a t_{acq} of 100 ms, $\frac{t_{delay}(\#5)}{T_1}$ = 21%, the difference between the first and fifth slices is ~22% at Ω = 0 which matches well with Eq. 4, and reduce to 3.2% at 7 ppm. Again, the T_1-relaxation effect can be corrected using Eq. 3 for the multi-slice spectra (Figure 3B). For CEST study, our approach relies on an accurate measure of S_{sat} (Ω = 0). When significant B_0-inhomogeneity is present, this data point can be obtained by interpolation and fitting of Z-spectrum, including the use of high order polynomials, or by a separate WASSR measurement. Alternatively, because the bandwidth of a

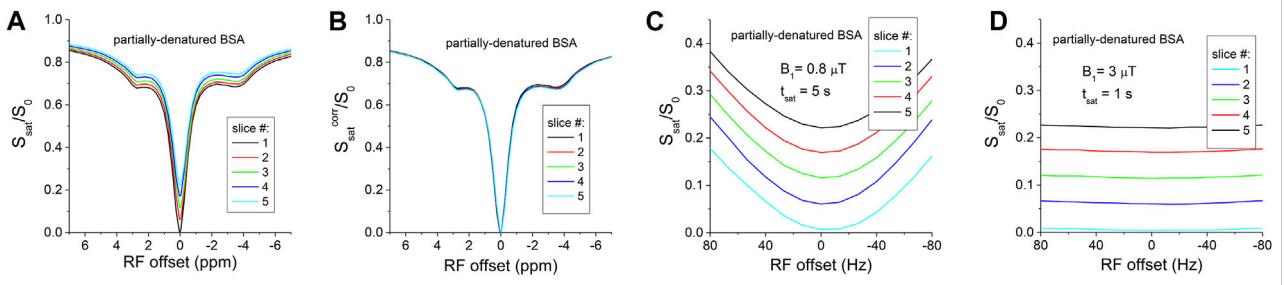

FIGURE 3
(A) Multi-slice Z-spectra of partially-denatured BSA shows the cross-slice T1-relaxation affects multiple signal contributions, including CEST, magnetization transfer (MT), NOE, and direct water saturation. **(B)** The cross-slice T1-relaxation can be satisfactorily corrected. The saturated signal near the water frequency is strongly dependent on the B_0 shift with a lower saturation power of 0.8 μT **(C)**, and becomes insensitive to the B_0 shift with a higher saturation power of 3 μT **(D)**.

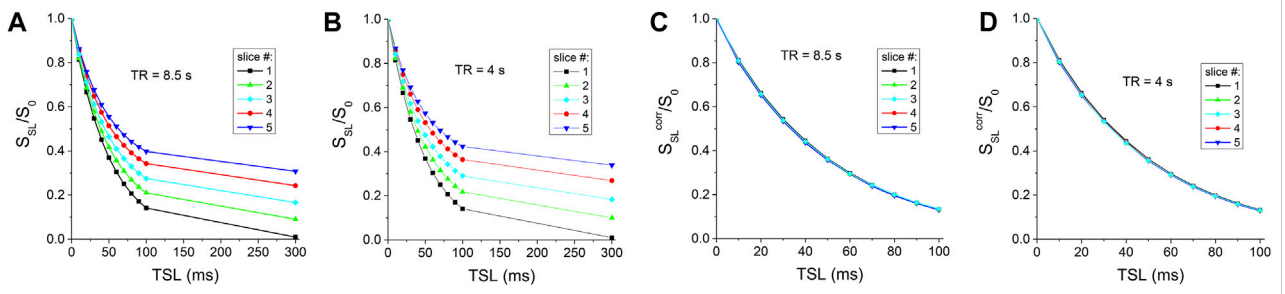

FIGURE 4
CESL signal as a function of TSL for **(A)** TR = 8.5 s and **(B)** TR = 4 s before and **(C,D)** after the correction of the cross-slice T_1-relaxation effect.

saturation pulse is correlated with the B_1 power, a high-power pulse can saturate the water signal for a wider B_0 range. Figure 3C indicated that for a saturation pulse of 0.8 μT and 5 s, there was significant variation in S_{sat} ($\Omega = 0$) of the heated BSA sample if the B_0 shift is large (e.g., >50 Hz). In contrast, the S_{sat} ($\Omega = 0$) is insensitive to the B_0 shift when a pulse of 3 μT and 1 s were used (Figure 3D).

In CESL experiments, the TSL-dependent signal of the BSA phantom is shown for TR = 8.5 s (Figure 4A). Similar to the CEST results, there is a clear T_1-relaxation effect for later slices. A mono-exponential fitting of the TSL-dependent data yields $T_{1\rho}$ value of 48.7 ms and 68.8 ms for the first and fifth slice, respectively. For a shorter TR = 4 s, the T_1-relaxation effect is slightly larger than that of TR = 8.5 s for later slices (Figure 4B), as shown by the signals at TSL = 300 ms. After a correction with Eq. 8, the TSL-dependent data overlaps well for both TR values (Figures 4C,D), and the fitted $T_{1\rho}$ value, averaged for the 5-slices, are 47.40 ± 0.75 ms and 47.38 ± 0.73 ms for TR = 8.5 s and 4 s, respectively, indicating good consistency.

Discussions

In CEST or CESL MRI, chemical exchange contrast can be affected by the T_1-relaxation between the irradiation preparation and the imaging module. The contamination is dependent on the ratio of t_{delay} and T_1, and thus, may be exacerbated at lower magnetic field strengths where T_1 is shorter. In this work, we reported a simple post-acquisition correction method with good accuracy. Multi-slice EPI was used as an example because the T_1-relaxation is minimal in the first slice, and thus, its first slice data can be used to determine the accuracy of the correction approach. Our approach only corrects the T_1-relaxation occurring between the irradiation pulse and the image acquisition, rather than the T_1-relaxation, if any, during the irradiation pulse. The CEST contrast competes with T_1 relaxation because the saturation transfer reduces the Z-magnetization of the water, whereas the T_1 relaxation brings the magnetization back to equilibrium. Therefore, the CEST effect is strongly affected by the water T_1, which is often corrected by a normalization of the water T_1 in CEST studies.

Besides EPI, imaging modules that have been used for CEST or CESL MRI include rapid acquisition with refocusing echoes (RARE), steady-state free precision (FISP), *etc.* In some of these imaging methods, there is a non-negligible delay between the end of saturation and the beginning of the central k-space even for a single slice imaging. For example, In FISP-CEST [37], the T_1-relaxation effect at the water resonance can be 10%–20% (as determined from the Z-spectrum signal at the water resonance frequency) for centric-encoding and even higher for linear-encoding, depending on the matrix size.

3D-CEST has recently been developed where the short saturation pulse and the imaging acquisition module are interleaved, so that the saturation reaches a steady state after a certain number of repetitions. Compare to multi-slice MRI, 3D acquisitions often require dedicated hardware for parallel imaging to speed up the acquisition. One drawback of this pulsed saturation approach is that the saturation frequency bandwidth is broader for shorter RF irradiation pulses which can affect the specificity of the CEST signal. Moreover, this approach has limitations because the optimal sensitivity for some CEST applications, such as those with a fast exchange, occurs with a relatively high power pulse at the transient state before reaching the steady-state.

This method is highly dependent on the accuracy of the correction term, i.e., the signal at 0 frequency offset for CEST or with long TSL for CESL. Thus, a high SNR for this correction image is critical. In addition, while correction methods that minimize the T_1-relaxation effect using specially designed irradiation schemes may be able to maintain CE contrast during acquisition [16, 32], post-acquisition correction such as the current method cannot artificially restore lost chemical exchange effects as the correction signal only contains T_1-information. Thus, our approach should only be applied to compensate for T_1-relaxation in cases where this relaxation has not fully diminished the chemical exchange contrast to noise ratio.

Although we only demonstrated our correction for CEST and CESL, this approach can be extended to other variants of chemical exchange sensitive MRI such as chemical exchange rotation transfer [38], on-resonance variable delay multiple pulse [39], or average saturation efficiency filter [40]. More generally, this method can also be applied to other imaging modalities where the imaging is acquired after a magnetization preparation and there is a delay between the preparation and the imaging module, such as multi-slice T_1-weighted imaging or diffusion-weighted imaging.

Conclusion

We reported a post-acquisition method to compensate for the T_1-relaxation effect in the CEST signal with multi-slice EPI imaging. This method is simple and easy to perform and can also be applied to other imaging modalities where there is a delay between the saturation and the imaging of the center k-space line.

Data availability statement

The raw data supporting the conclusion of this article will be made available by the authors, without undue reservation.

Author contributions

TJ derived the formula, designed the experiment, performed part of the experiments, and write the manuscript. JC performed part of the experiments and manuscript writing.

Funding

This work is supported by NIH grant NS100703.

Conflict of interest

The authors declare that the research was conducted in the absence of any commercial or financial relationships that could be construed as a potential conflict of interest.

Publisher's note

All claims expressed in this article are solely those of the authors and do not necessarily represent those of their affiliated organizations, or those of the publisher, the editors and the reviewers. Any product that may be evaluated in this article, or claim that may be made by its manufacturer, is not guaranteed or endorsed by the publisher.

References

1. Ward KM, Aletras AH, Balaban RS. A new class of contrast agents for MRI based on proton chemical exchange dependent saturation transfer (CEST). *J Magn Reson* (2000) 143(1):79–87. doi:10.1006/jmre.1999.1956

2. Zhang SR, Merritt M, Woessner DE, Lenkinski RE, Sherry AD. PARACEST agents: Modulating MRI contrast via water proton exchange. *Acc Chem Res* (2003) 36(10):783–90. doi:10.1021/ar020228m

3. van Zijl PCM, Yadav NN. Chemical exchange saturation transfer (CEST): What is in a name and what isn't? *Magn Reson Med* (2011) 65(4):927–48. doi:10.1002/mrm.22761

4. Jin T, Wang P, Zong X, Kim SG. Magnetic resonance imaging of the Amine-Proton EXchange (APEX) dependent contrast. *Neuroimage* (2012) 59(2):1218–27. doi:10.1016/j.neuroimage.2011.08.014

5. Jin T, Wang P, Zong X, Kim SG. MR imaging of the amide-proton transfer effect and the pH-insensitive nuclear overhauser effect at 9.4 T. *Magn Reson Med* (2013) 69(3):760–70. doi:10.1002/mrm.24315

6. Chung JJ, Jin T, Lee JH, Kim SG. Chemical exchange saturation transfer imaging of phosphocreatine in the muscle. *Magn Reson Med* (2019) 81(6):3476–87. doi:10.1002/mrm.27655

7. Zong X, Wang P, Kim S-G, Jin T. Sensitivity and source of amine-proton exchange and amide-proton transfer magnetic resonance imaging in cerebral ischemia. *Magn Reson Med* (2014) 71(1):118–32. doi:10.1002/mrm.24639

8. Jin T, Wang P, Hitchens TK, Kim SG. Enhancing sensitivity of pH-weighted MRI with combination of amide and guanidyl CEST. *Neuroimage* (2017) 157: 341–50. doi:10.1016/j.neuroimage.2017.06.007

9. Jin T, Iordanova B, Hitchens TK, Modo M, Wang P, Mehrens H, et al. Chemical exchange-sensitive spin-lock (CESL) MRI of glucose and analogs in brain tumors. *Magn Reson Med* (2018) 80(2):488–95. doi:10.1002/mrm.27183

10. Zhou JY, Payen JF, Wilson DA, Traystman RJ, van Zijl PCM. Using the amide proton signals of intracellular proteins and peptides to detect pH effects in MRI. *Nat Med* (2003) 9(8):1085–90. doi:10.1038/nm907

11. Zhou JY, Tryggestad E, Wen ZB, Lal B, Zhou T, Grossman R, et al. Differentiation between glioma and radiation necrosis using molecular magnetic resonance imaging of endogenous proteins and peptides. *Nat Med* (2011) 17(1): 130–4. doi:10.1038/nm.2268

12. Zhou JY, Blakeley JO, Hua J, Kim M, Laterra J, Pomper MG, et al. Practical data acquisition method for human brain tumor amide proton transfer (APT) imaging. *Magn Reson Med* (2008) 60(4):842–9. doi:10.1002/mrm.21712

13. Chan KWY, McMahon MT, Kato Y, Liu G, Bulte JWM, Bhujwalla ZM, et al. Natural D-glucose as a biodegradable MRI contrast agent for detecting cancer. *Magn Reson Med* (2012) 68(6):1764–73. doi:10.1002/mrm.24520

14. Sun PZ, Zhou JY, Sun WY, Huang J, van Zijl PCM. Detection of the ischemic penumbra using pH-weighted MRI. *J Cereb Blood Flow Metab* (2007) 27(6): 1129–36. doi:10.1038/sj.jcbfm.9600424

15. Sun PZ, Sorensen AG. Imaging pH using the chemical exchange saturation transfer (CEST) MRI: Correction of concomitant RF irradiation effects to quantify CEST MRI for chemical exchange rate and pH. *Magn Reson Med* (2008) 60(2): 390–7. doi:10.1002/mrm.21653

16. Sun PZ, Cheung JS, Wang EF, Benner T, Sorensen AG. Fast multislice pH-weighted chemical exchange saturation transfer (CEST) MRI with unevenly segmented RF irradiation. *Magn Reson Med* (2011) 65(2):588–94. doi:10.1002/mrm.22628

17. Haris M, Singh A, Cai K, Nath K, Crescenzi R, Kogan F, et al. Micest: A potential tool for non-invasive detection of molecular changes in alzheimer's disease. *J Neurosci Methods* (2013) 212(1):87–93. doi:10.1016/j.jneumeth.2012.09.025

18. Haris M, Cai K, Singh A, Hariharan H, Reddy R. *In vivo* mapping of brain myo-inositol. *Neuroimage* (2011) 54(3):2079–85. doi:10.1016/j.neuroimage.2010.10.017

19. Chen L, Wei ZL, Chan KWY, Cai S, Liu G, Lu H, et al. Protein aggregation linked to Alzheimer's disease revealed by saturation transfer MRI. *Neuroimage* (2019) 188:380–90. doi:10.1016/j.neuroimage.2018.12.018

20. Longo DL, Dastru W, Digilio G, Keupp J, Langereis S, Lanzardo S, et al. Iopamidol as a responsive MRI-chemical exchange saturation transfer contrast agent for pH mapping of kidneys: *In vivo* studies in mice at 7 T. *Magn Reson Med* (2011) 65(1):202–11. doi:10.1002/mrm.22608

21. Vinogradov E, He HM, Lubag A, Balschi JA, Sherry AD, Lenkinski RE. MRI detection of paramagnetic chemical exchange effects in mice kidneys *in vivo*. *Magn Reson Med* (2007) 58(4):650–5. doi:10.1002/mrm.21393

22. Chen L, Barker PB, Weiss RG, van Zijl PCM, Xu JD. Creatine and phosphocreatine mapping of mouse skeletal muscle by a polynomial and Lorentzian line-shape fitting CEST method. *Magn Reson Med* (2019) 81(1): 69–78. doi:10.1002/mrm.27514

23. Haris M, Nanga RPR, Singh A, Cai K, Kogan F, Hariharan H, et al. Exchange rates of creatine kinase metabolites: Feasibility of imaging creatine by chemical exchange saturation transfer MRI. *NMR Biomed* (2012) 25(11):1305–9. doi:10.1002/nbm.2792

24. Rerich E, Zaiss M, Korzowski A, Ladd ME, Bachert P. Relaxation-compensated CEST-MRI at 7T for mapping of creatine content and pH - preliminary application in human muscle tissue *in vivo*. *NMR Biomed* (2015) 28(11):1402–12. doi:10.1002/nbm.3367

25. Pavuluri K, Manoli I, Pass A, Li Y, Vernon HJ, Venditti CP, et al. Noninvasive monitoring of chronic kidney disease using pH and perfusion imaging. *Sci Adv* (2019) 5(8):eaaw8357. doi:10.1126/sciadv.aaw8357

26. Jin T, Autio J, Obata T, Kim SG. Spin-locking versus chemical exchange saturation transfer MRI for investigating chemical exchange process between water and labile metabolite protons. *Magn Reson Med* (2011) 65(5):1448–60. doi:10.1002/mrm.22721

27. Jin T, Kim SG. Advantages of chemical exchange-sensitive spin-lock (CESL) over chemical exchange saturation transfer (CEST) for hydroxyl–and amine-water proton exchange studies. *NMR Biomed* (2014) 27:1313–24. doi:10.1002/nbm.3191

28. Yuan J, Zhou JY, Ahuja AT, Jwang YX. MR chemical exchange imaging with spin-lock technique (CESL): A theoretical analysis of the Z-spectrum using a two-pool R-1 rho relaxation model beyond the fast-exchange limit. *Phys Med Biol* (2012) 57(24):8185–200. doi:10.1088/0031-9155/57/24/8185

29. Jiang BY, Jin T, Blu T, Chen WT. Probing chemical exchange using quantitative spin-lock R-1 rho asymmetry imaging with adiabatic RF pulses. *Magn Reson Med* (2019) 82(5):1767–81. doi:10.1002/mrm.27868

30. Jin T, Mehrens H, Hendrich K, Kim SG. Mapping brain glucose uptake with chemical exchange-sensitive spin-lock magnetic resonance imaging. *J Cereb Blood Flow Metab* (2014) 34(8):1402–10. doi:10.1038/jcbfm.2014.97

31. Sun PZ, Murata Y, Lu J, Wang X, Lo EH, Sorensen AG. Relaxation-Compensated fast multislice amide proton transfer (APT) imaging of acute ischemic stroke. *Magn Reson Med* (2008) 59:1175–82. doi:10.1002/mrm.21591

32. Villano D, Romdhane F, Irrera P, Consolino L, Anemone A, Zaiss M, et al. A fast multislice sequence for 3D MRI-CEST pH imaging. *Magn Reson Med* (2021) 85(3):1335–49. doi:10.1002/mrm.28516

33. Li XJ, Han ET, Ma CB, Link TM, Newitt DC, Majumdar S. *In vivo* 3T spiral imaging based multi-slice T1ρ mapping of knee cartilage in osteoarthritis. *Magn Reson Med* (2005) 54(4):929–36. doi:10.1002/mrm.20609

34. Jin T. Post-acquisition correction of the T1 relaxation effect for fast multi-slice CEST MRI. In: Proceedings of 28th Annual Meeting of ISMRM2020; Virtual conference (2022).

35. Jin T, Mehrens H, Wang P, Kim SG. Chemical exchange-sensitive spin-lock MRI of glucose analog 3-O-methyl-d-glucose in normal and ischemic brain. *J Cereb Blood Flow Metab* (2017) 38:869–80. doi:10.1177/0271678x17707419

36. Zu Z, Li H, Jiang X, Gore JC. Spin-lock imaging of exogenous exchange-based contrast agents to assess tissue pH. *Magn Reson Med* (2018) 79(1):298–305. doi:10.1002/mrm.26681

37. Shah T, Lu L, Dell KM, Pagel MD, Griswold MA, Flask CA. CEST-FISP: A novel technique for rapid chemical exchange saturation transfer MRI at 7 T. *Magn Reson Med* (2011) 65(2):432–7. doi:10.1002/mrm.22637

38. Zu ZL, Li H, Xu JZ, Zhang XY, Zaiss M, Li K, et al. Measurement of APT using a combined CERT-AREX approach with varying duty cycles. *Magn Reson Imaging* (2017) 42:22–31. doi:10.1016/j.mri.2017.05.001

39. Xu X, Xu JD, Chan KWY, Liu J, Liu H, Li Y, et al. GlucoCEST imaging with on-resonance variable delay multiple pulse (onVDMP) MRI. *Magn Reson Med* (2019) 81(1):47–56. doi:10.1002/mrm.27364

40. Jin T, Chung JJ, et al. Average saturation efficiency filter (ASEF) for CEST imaging. *Magn Reson Med* (2022) 88(1):254–265. doi:10.1002/mrm.29211